

520-34  
52185

# NON-ISOTHERMAL EXPERIMENTAL STUDY OF THE CONSTRAINED VAPOR BUBBLE THERMOSYPHON

68

Muthu Karthikeyan, Jianming Huang, Joel Plawsky, and Peter Wayner, Jr.  
The Isermann Department of Chemical Engineering  
Rensselaer Polytechnic Institute  
Troy, New York 12180-3590

## ABSTRACT

Experimental and theoretical techniques to study non-isothermal transport processes in the constrained vapor bubble thermosyphon (CVBT) were developed using a pentane/quartz system. The transport processes can be evaluated by measuring the liquid film profile, which gives the pressure field, and the temperature field. The axial variation in the capillary pressure was measured using an image-analyzing interferometer that is based on computer-enhanced video microscopy of the naturally occurring interference fringes. Thermoelectric coolers were used to control the temperature level in the condensation region and, therefore, the length of the approximately "adiabatic" surface region which is a function of the temperature difference between the CVBT surface and the surroundings. High values for the axial thermal conductance in the "adiabatic" surface region were demonstrated under certain conditions.

## INTRODUCTION

In order to study the details of transport processes in heat pipes, we report on our investigation of a larger version of Cotter's micro heat pipe (1) in the form of a 3 x 3 x 40 mm fused quartz cell of square cross-section. In this case, the capillary driving force in a portion of the cell is of the same order of magnitude as the gravity force unlike a micro heat pipe for which the capillary force is sometimes much larger than the gravity force. Hence, we call this cell a Constrained Vapor Bubble Thermosyphon (CVBT). From a fundamental point of view, the CVBT conveniently permits the study of interfacial transport concepts. In particular, we are concerned with the experimental study of the generic CVBT presented in Fig. 1 for a micro-gravity environment. For a completely wetting system, the liquid will coat all the walls of the chamber. For a finite contact angle system, some of the walls will have only a small amount of adsorbed vapor that changes the surface properties at the solid-vapor interface. Liquid will fill a portion of the corners in both cases. If temperature at End (2) is higher than End (1) because of an external heat source, energy flows from End (2) to End (1) by conduction in the walls and by a combined evaporation, vapor flow, and condensation mechanism. Heat applied to End (2) vaporizes the liquid in this region and the vapor is forced to move to End (1) where it condenses, releasing the latent heat of vaporization in the process. The curvature of the liquid-vapor interface changes continually along the cell because of viscous losses, and the vaporization/condensation process. This capillary pressure difference between the evaporator and the condenser regions causes the working fluid to flow back to End(2) from End(1) along the right-angled corner regions. These corner regions act as liquid arteries and hence replace the wicking structure of a conventional heat pipe. Herein, we present the results of our initial ground-based non-isothermal studies which are a prologue to micro-gravity studies.

In order for the CVBT to operate, the maximum available capillary pumping head must be greater than the total pressure drop in the CVBT in a gravitational field. This pressure drop is made up of three components: The pressure drop  $\Delta P_l$  required to return the liquid from the condenser to the evaporator; The pressure drop  $\Delta P_v$  necessary to cause the vapor to flow from

the evaporator to the condenser ; The gravitational head  $\Delta P_g$  which may be zero, positive or negative.

$$(\Delta P_c)_{\max} \geq \Delta P_l + \Delta P_v + \Delta P_g \quad (1)$$

where the difference between the augmented Young-Laplace equations at locations (2) and (1) is

$$(\Delta P_c) = \sigma_l \left[ \frac{1}{r_{c_2}} - \frac{1}{r_{c_1}} \right] + \Pi_2 - \Pi_1 \quad (2)$$

The first term accounts for the change in the capillary force and  $\Pi$  is the disjoining pressure. A discussion concerning the use of this equation for the shape dependent stress field is given by DasGupta, et al. (2). In general, the performance of the CVBT is based on the chemical potential profile, which is a function of the temperature and pressure profiles. The pressure profile is connected to the film thickness profile by the augmented Young-Laplace equation, Eq. (2). Therefore, we need to measure the temperature and thickness profiles.

## EXPERIMENTAL PROCEDURE AND OBSERVATIONS

The CVBT experimental setup consists mainly of the quartz cell, a resistance heater, and four miniature (5 x 5 x 2.4mm) thermoelectric coolers. The heater was a hollow cylinder of *Garrolite* approximately 60 mm long on which high-resistivity nichrome wire was tightly wound. A 4.76 mm diameter, stainless steel rod of 85 mm length was inserted into the heater in such a way that 25 mm of the rod projected out of one end of the heater. The contact resistance between the heater and the stainless steel rod was reduced by using a layer of thermally conductive paste between the contact surfaces. The projecting end of the stainless steel rod was then attached to the cell using high thermal conductivity silver epoxy. The heater and the projected portion of the rod were thoroughly insulated to minimize heat loss. This arrangement enables us to estimate the heat input into the cell by measuring the temperature profile of the stainless steel rod. A simple fin equation can then be fitted to the temperature data to yield the rate of heat transport from the end of the rod to the cell. The whole assembly was mounted on the mechanical stage of a high-power light microscope. This enables the movement of the assembly on the stage so that any part of the cell could be viewed under the microscope, and the liquid film thickness profile measured at that location. The pentane (99.9% purity) working fluid used in the vapor bubble thermosyphon experiments was de-aerated and stripped of higher boiling substances by a single vacuum distillation step.

The temperature profiles of both the rod and the quartz cell were measured using closely spaced micro-scale (40 AWG) Chromel-Alumel thermocouple beads. These were attached to the side of the cell and the rod using conductive silver epoxy and the beads were then coated with regular epoxy to reduce the error in the measured temperature due to the effect of the surroundings. The coolers were firmly pressed against the edges of end (1) of the cell. A thin coating of thermally conductive paste ensures good thermal contact between the cell and the coolers. It should be pointed out that, although the coolers were primarily designed to help retain the bubble within the cell by maintaining a constant low temperature at the cooler end, they were found to have an additional important function. We found that the length of the adiabatic region could be changed by using the coolers to lower the temperature in the middle portion of the cell to a value close to that of the surroundings. A drawing of a corner of the CVBT, where the thickness profile was measured, is presented in Fig. 2. Details of this film thickness measurement, known as Image Analyzing Interferometry (IAI) are elaborated elsewhere

(DasGupta, 1995). The cell had roughly 40 to 50% of liquid by volume while the remaining volume was occupied by pentane vapor. We established the vapor bubble at the heater end by slightly tilting the setup in such a way that liquid flowed out of the heated end.

Prior to the experiments, the CVBT cell and the connecting tubes were thoroughly cleaned in an ultrasonic bath and dried in an oven. The cell alone was rinsed for 1 minute with a dilute (1%) solution of Hydrofluoric acid to remove a thin layer of quartz along with the contaminants adhering to the surface. This proved quite effective although it rendered the inner surface of the cell considerably rougher than it was before. A final rinse with de-ionized water was performed and the cell was blow dried in a stream of ultra-clean, dry nitrogen. The cell was attached to the liquid feeder/vacuum assembly by means of heat shrink Teflon tubing. The whole assembly was evacuated and a sufficient amount of pentane was distilled into the cell from the holding Squibb funnel. The pressure inside the system was continuously monitored using an *Omega* Pressure transducer/Digital meter combination, to ensure the lack of contamination by air.

### EXPERIMENTAL RESULTS AND DISCUSSION

Figure 3 shows a plot of the temperature difference between the surface of the CVBT and the room,  $\theta$  versus the axial distance,  $x$ , for a CVBT and the corresponding dry quartz cell. The electrical power input to the heater was 1.5 W in both cases. The difference between the two profiles is not dramatic because the coolers at the end of the CVBT remained off during the course of these experiments. Data presented below for different heater and cooler power settings indicate that a flat temperature profile in the middle of the CVBT could be obtained for a particular combination of these power settings.

The stainless steel rod was designed to evaluate the heat input into both the CVBT and the dry cell. The measured steel rod temperatures were fitted to the following fin solution equation, with the overall effective heat transfer coefficient  $U$  between the steel rod and the environment evaluated as a variable parameter.

$$\frac{\theta}{\theta_b} = \frac{(\theta_s / \theta_b) \sinh mx + \sinh m(l_s - x)}{\sinh ml_s} \quad (3)$$

where  $\theta_s$  and  $\theta_b$  are the temperature differences between the CVBT and the room at the beginning and at the thermocouple location just before the end of the stainless steel rod. For the purposes of this analysis, the temperature differential at the end of the steel rod (at the interface between the rod and the cell) was omitted since this reading might not be accurate.  $l_s$  is the distance between the first and the last measured points used for calculation, which in this case is 20 mm, and  $m$  is defined by the following equation.

$$m^2 = \frac{UP}{kA_c} \quad (4)$$

where  $P$ ,  $k$ , and  $A_c$  are the perimeter, the thermal conductivity and the cross-sectional area of the stainless steel rod, respectively. Least squares method was used to obtain  $U$  from the best fit of the data. Then, the heat going out from the end of the steel rod,  $Q_{out}$ , was calculated from the fin equation.

Sets of CVBT experiments and corresponding dry cell experiments (same  $Q$  in both cases) were run at different heater power inputs. Using the same  $Q$ , a fin solution was obtained for a hypothetical solid quartz rod of similar length and cross-sectional area. The results for these

three cases are compared in Fig. 4 for  $Q=0.1$  W. As seen from this figure, the dry cell data can also be modeled as a fin with an appropriate value for the heat transfer coefficient,  $h$ . It is obvious that, for  $Q=0.1$  W, the CVBT has the lowest resistance. The local heat flux was calculated as follows: First, the heat transfer coefficient,  $h$  was calculated by fitting the dry cell data to a fin equation. Then, the local axial heat flux at different locations in the CVBT were calculated using the following equation:

$$q(x) = \frac{Q - \int_0^x Ph\theta dx}{A} \quad (5)$$

where  $Q$  is the heat input to the CVBT,  $P$  the perimeter of the CVBT and  $A$  the cross-sectional area of the CVBT. Assuming that the value of the heat transfer coefficient between the surface of the CVBT and the room,  $h$ , is equal to the value obtained with the dry cell at approximately the same temperature, the surface heat flux was obtained. The integration was performed numerically with the cubic spline fit data. We found that, in this case, the heat rate from the CVBT obtained through integration of the temperature of the CVBT equaled the heat input  $Q$  to within 1%. The temperature profile of the CVBT in Fig. 4 was fitted as a smoothed cubic spline and the local slopes of the profile  $d\theta/dx$  were obtained numerically. Therefore, the local effective thermal conductivity can be obtained using the equation below:

$$k_{eff}(x) = -\frac{q(x)}{\frac{d\theta}{dx}(x)} \quad (6)$$

The local effective thermal conductivity distribution in the CVBT, with coolers off for  $Q=0.1$  W is shown in Fig. 5. As seen, the local heat flux decreases along the cell. But the effective thermal conductivity goes through a maximum value in the middle of the cell where the slope of the temperature profile becomes very small. For this portion of the CVBT, the effective thermal conductivity is comparable to that of the stainless steel rod. The results presented next demonstrate that the performance can be dramatically improved by using the thermoelectric coolers. Experiments with the coolers on at the end of the CVBT were also conducted. A comparison of two cases, one with the coolers on and the other with the coolers off, is presented in Fig. 6. We find that, for the same power input to the heater, a CVBT with coolers to remove the heat from the end performs much better (higher  $k_{eff}$ ) than the one with only natural convection to remove the heat. Also, the CVBT with the coolers on has a long distinct horizontal temperature region and a smaller base temperature. It is obvious that the efficiency of the CVBT reaches the maximum in this region. In essence, we were able to expand the "adiabatic" length by lowering  $\theta$ .

If the vapor pressure gradient is negligible, the liquid pressure gradient is due to the curvature gradient.

$$\frac{dP_l}{dP_x} = -\sigma_l \frac{dK}{dx} \quad (7)$$

As mentioned earlier, the liquid film thickness measurements were carried out. A plot of the curvature distribution of CVBT(coolers off) for  $Q=0.1$  W is shown in Fig. 7. This figure shows that the curvature decreases from the high temperature region to the low temperature region. Although, the analysis and data are incomplete, a rough calculation shows that this curvature gradient gives the correct order of magnitude for  $Q$ .

## CONCLUSIONS

Based on the experiments and subsequent analysis of the data gathered we reach the following conclusions:

1. Experimental and theoretical techniques to study non-isothermal transport processes in the constrained vapor bubble thermosyphon(CVBT) were developed.
2. The transport processes can be evaluated by measuring the liquid film profile using an image-analyzing interferometer, which gives the pressure field, and the temperature field.
3. Thermoelectric coolers can be used to *control* the temperature level in the condensation region and, therefore, the length of the approximately "adiabatic" surface region.
4. High values for the axial thermal conductance in the "adiabatic" surface region were demonstrated under certain conditions.

## ACKNOWLEDGMENT

This material is based on work supported by the National Aeronautics and Space Administration under grant # NAG3-1399. Any opinions, findings, and conclusions or recommendations expressed in this publication are those of the authors and do not necessarily reflect the view of NASA.

## REFERENCES

1. Cotter, T. P., 1984, "Principles and Prospects of Micro Heat Pipes", Proc 5th Int Heat Pipe Conf, Tsukuba, Japan, pp. 328-335.
2. DasGupta, S., Plawsky, J. L., and Wayner, P. C., Jr., 1995, "Interfacial Force Field Characterization in a Constrained Vapor Bubble Thermosyphon", AIChE Journal, 41(9), pp. 2140-2149.

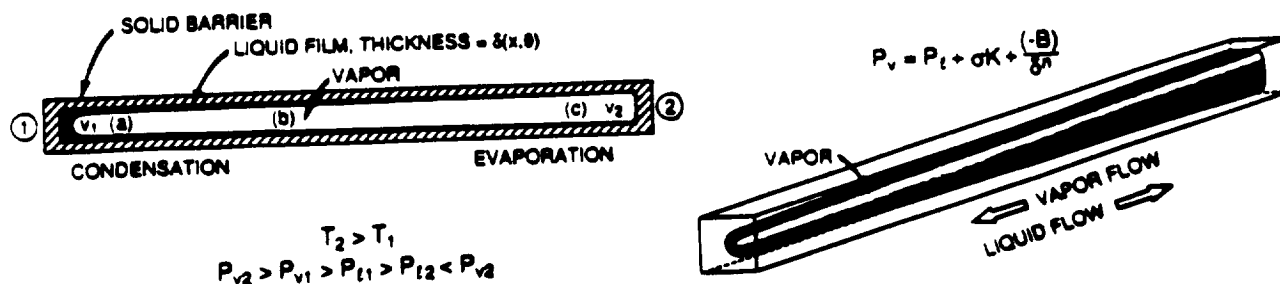


Figure 1. Constrained Vapor Bubble Thermosyphon Concept.

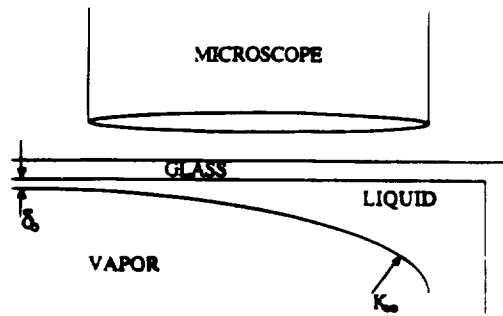


Figure 2. Location of microscope.

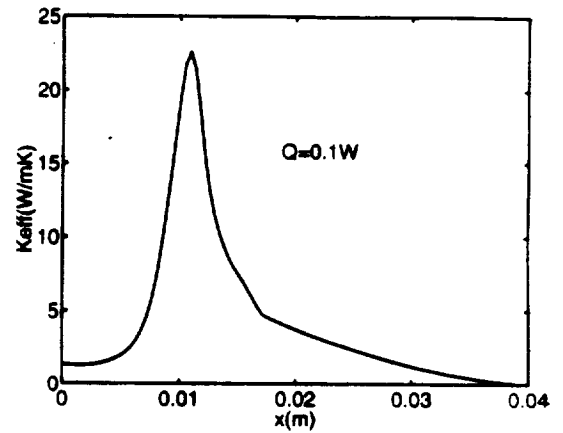


Figure 5. Local axial effective thermal conductivity distribution in CVBT for  $\theta(x)$  given in Figure 4.

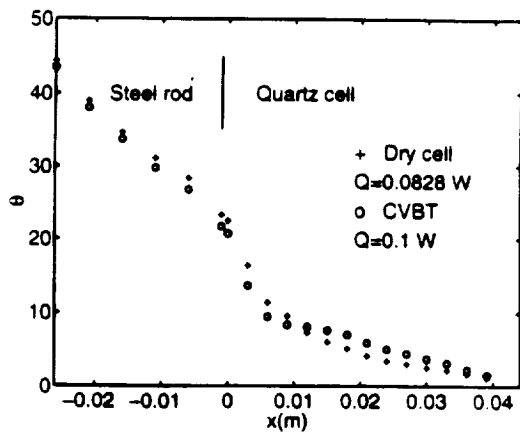


Figure 3. Comparison of  $\theta$  profile for CVBT and dry cell.

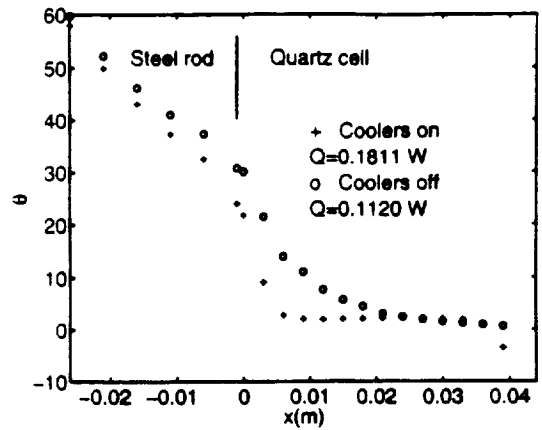


Figure 6. Comparison of CVBT with or without cooler on at same power input to heater, 2.2W.

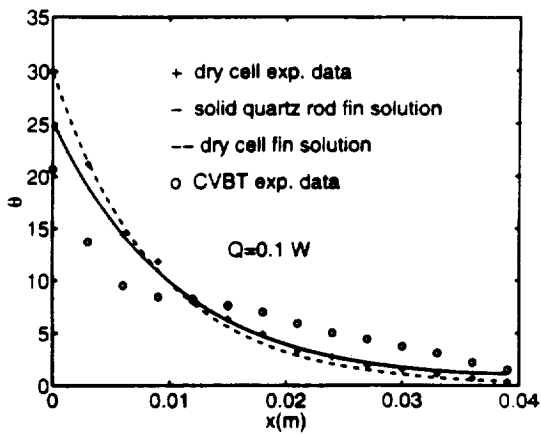


Figure 4. Comparison of the  $\theta$  profiles for the CVBT (coolers off), dry cell and solid quartz rod.

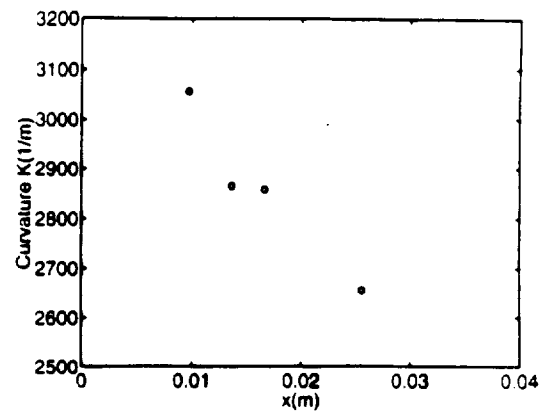


Figure 7. Curvature distribution in CVBT for data given in Figure 4 ( $Q=0.1$  W, coolers off).